Resonant excitation channels in the $3d^{10}$-$3d^94s$ and $3d^{10}$-$3d^94p$ transitions of nickel-like Mo^{14+} and Zr^{12+}

K. B. Fournier* and W. H. Goldstein
Lawrence Livermore National Laboratories, P.O. Box 808, Livermore, California 94550

M. May and M. Finkenthal†
Department of Physics and Astronomy, The Johns Hopkins University, Baltimore, Maryland 21218

J. L. Terry
Plasma Fusion Center, Massachusetts Institute of Technology, Cambridge, Massachusetts 02139-4307

(Received 17 October 1995)

At energies below the threshold for direct electron impact excitation, resonant excitations can make a significant contribution to the total excitation rate of a given energy level. In this paper, the rates of resonant excitation into the levels of the $3d^94s$ and $3d^94p$ configurations of Mo^{14+} have been calculated using a fully relativistic, multiconfiguration atomic structure code and detailed accounting of energy levels. By including the effects of resonant excitations in collisional-radiative models for the spectrum of Ni I–like Mo^{14+} and (by isoelectronic scaling) Zr^{12+}, the ratio of the emissivity of the $3d^{10}$-$4d^94s$ $E2$ transitions to the emissivity of the $3d^{10}$-$3d^94p$ $E1$ transitions is greatly enhanced, and sensitivity to electron temperature in the ratio is introduced. This ratio is density sensitive for $n_e \geqslant 10^{13}$ cm^{-3}, and therefore, given knowledge of either local temperature or density conditions, the $E2$-$E1$ ratio can serve as a diagnostic for local conditions in magnetically confined fusion plasmas. The current work demonstrates the need to include resonant excitations in collisional-radiative models of the soft x-ray emission of nickel-like ions. Good agreement is found between measurements of $E1$ and $E2$ line brightness ratios made in a tokamak plasma, and the predictions of collisional-radiative models in the present work.

PACS number(s): 32.70.Fw, 52.25.Vy, 32.80.Dz

I. INTRODUCTION

The Ni I–like ion, with its filled $3d$ shell ground state has a much higher ionization potential than adjacent N-shell isosequences. Consequently, the Ni I–like ion will be far more abundant in a fusion plasma than the Cu I– or Zn I–like ions. This characteristic makes the Ni I–like ion a valuable tool for diagnosing local plasma conditions [1]. Elements in the Ni I–like isosequence are also important for the lasing transitions that occur between the (metastable) $3d^94d$ and $3d^94p$ levels [2,3]. The nickel-like charge state of refractory metals (zirconium to silver) can exist in low-density plasmas at temperatures of a few hundred electron-volts or less. The use of refractory metals in magnetically confined fusion devices means the nickel-like charge state will be an unambiguous radiator in the outer part of the plasma, where the appropriate temperatures obtain. It is well known for the Ne I–like isosequence that at temperatures below the excitation threshold for transitions from the ground state to low-lying excited states, radiationless capture of a free electron followed by autoionization can greatly enhance the total excitation rate [4]. In the present work, resonant excitation channels are found to have a large contribution to the $3d$-$4s$ and $3d$-$4p$ excitation rates in Ni I–like Mo^{14+} and Zr^{12+}.

The $3d^{10}$-$3d^94p$ $E1$ lines for Mo^{14+} have been identified in vacuum spark [5], tokamak [6], and laser-produced plasmas [7]. The $3d^{10}$-$3d^94s$ $E2$ lines from Mo^{14+} were measured and classified by Mansfield *et al.* in a tokamak plasma [8]. Identification of the Mo^{14+} $3d$-$4s$ $E2$ lines and models for the electron density dependence of the ratio of the emissivity of the $3d$-$4s$ $E2$ and $3d$-$4p$ $E1$ lines have been published by Klapisch *et al.* in Ref. [1]. For a picture of the Mo^{14+} spectrum, see Fig. 4 in Ref. [1]. Zr^{12+} emission features are less well known; the $3d^{10}$-$3d^94p$ $E1$ lines were measured in a vacuum-spark plasma by Alexander *et al.* [5] over two decades ago. To the best of our knowledge, until now, no observations have been reported of the $3d$-$4s$ $E2$ lines in Zr^{12+}.

In Sec. II we present the calculation of resonant-excitation rates into the $3d^94l$ ($l=s,p$) levels of Mo^{14+}. In Sec. III, we report on observations of the Mo^{14+} $E2$-$E1$ ratio made in a tokamak plasma and compare them to models that include the resonant contribution to the $E2$ and $E1$ transitions. We then present observations of the $3d^{10}$-$3d^94s$ Zr^{12+} (and $3d^9$-$3d^84s$ Zr^{13+} $E2$) lines and compare the observed Ni I–like zirconium transitions with models of the Zr^{12+} $E2$-$E1$ ratio. In general, good agreement is found.

II. RESONANT EXCITATION PROCESSES

The resonant excitation (RX) process involves the radiationless capture of a free electron by the ground state of the

*Also at Department of Physics and Astronomy, The Johns Hopkins University.

†Permament address: Racah Institute of Physics, The Hebrew University, Jerusalem, Israel.

initial ion, e.g., Mo^{14+}. The resulting doubly excited state of Mo^{13+} (Cu I–like) can deexcite in several ways. If it autoionizes to an excited state of Mo^{14+}, the two-step process is a resonant enhancement of direct excitation [4]. The rate at which population is excited into a level j of Mo^{14+} through RX is given in the isolated resonance approximation by

$$Q_j^{\mathrm{RX}}=\frac{1}{2g_i}\left(\frac{4\pi a_0^2 Ry}{kT}\right)^{3/2}\sum_d g_d \exp\left(-\frac{E_d}{kT}\right)A_d^{\mathrm{Auger}}B_{d,j}^{A}, \tag{1}$$

where g_i is the multiplicity of the initial state of Mo^{14+}, d denotes a doubly excited state of Mo^{13+}, g_d is its multiplicity, A_d^{Auger} is the rate for autoionizing (Auger) transitions, a_0 is the Bohr radius, E_d is the capture energy, and the branching ratio for autoionization to level j is

$$B_{d,j}^{A}=\frac{A_{d,j}^{\mathrm{Auger}}}{\Sigma_f A_{d,f}^{\mathrm{rad}}+\Sigma_f A_{d,f}^{\mathrm{Auger}}}. \tag{2}$$

Ab initio computations of energy levels and radiative and Auger transition probabilities were performed using the relativistic structure code RELAC [9,10]. For the sum over Auger channels in the branching ratio, Eq. (2), the 35 levels of Mo^{14+} from the $3d^{10}$, $3d^9 4s$, $3d^9 4p$, and $3d^9 4d$ configurations were included as final states. The states of Mo^{13+} considered through which the RX process can proceed are

$$3p^6 3d^9 4ln'l' \quad (l\leqslant 3; 5\leqslant n'\leqslant 12, l'\leqslant 5)$$

$$3p^5 3d^{10} 4ln'l' \quad (l\leqslant 3; 4\leqslant n'\leqslant 10, l'\leqslant 5).$$

The calculations for the level energies of the Mo^{14+} states include configuration interaction (CI) in all the above-listed configurations. For the $3p^6 3d^9 4ln'l'$ states, for all values of l simultaneously, the levels of a fixed n' and all possible values of l' were allowed to interact. For the $3p^5 3d^{10} 4ln'l'$ levels, configuration interaction has been limited to all levels formed from a fixed value of l and n' for all possible values of l'.

Radiative decays from the doubly excited states of Mo^{13+} to all possible states above and below the continuum have been included in the present calculations. When a stabilizing transition is forbidden, radiative decays between the levels of Mo^{13+} above the continuum may contribute some tens of percents to the total width for radiative decays from a particular configuration in the sum over Einstein coefficients in Eq. (2). Transitions by a valence electron (e.g., $3p^6 3d^9 4d5g \rightarrow 3p^6 3d^9 4d5f$), and transitions by a core electron in the doubly excited states of Mo^{13+} (e.g., $3p^5 3d^{10} 4pn'l' \rightarrow 3p^6 3d^9 4pn'l'$), result in final states that can autoionize; in this case, the effect of cascades on the branching ratio described by Eq. (2) has been included. Because of the fast rates for the dominant stabilizing transitions, the effect of cascades on the total RX rate into each level of Mo^{14+} is small.

The RX rate coefficients, along with the direct, DWA collisional excitation rate coefficients for the four $3d^9 4s$ and twelve $3d^9 4p$ levels of Mo^{14+} are listed in Table I. A plot of the RX rate coefficient versus temperature for eight of the excited levels of Mo^{14+} is shown in Fig. 1. The factor by which the resonant excitation channels enhance the direct, impact-excitation rate from the ground state is shown as a function of temperature for four Mo^{14+} levels in Fig. 2. The quantity that is plotted is the sum of the resonant excitation rate and the direct, impact-excitation rate, divided by the direct, impact-excitation rate. The levels shown in Fig. 2 are identified in Table I.

The running sum of the explicitly calculated contribution to the total RX rate coefficient of each manifold of levels formed from each value of n' (summed over all values of l and l') for both the $3d$-$4l$ and $3p$-$4l$ excitation channels for four different Mo^{14+} levels is shown in Fig. 3. The flatness of the sum with each new manifold indicates that the calculation has converged. In the cases where the running sum has not converged, a n^{-3} scaling has been used to continue the sums until convergence is achieved.

III. OBSERVATIONS AND DISCUSSION

Spectra of Mo^{14+} and Zr^{12+} have been experimentally obtained from the Alcator C-Mod Tokamak at the Massachusetts Institute of Technology (MIT) [11]. Two series of reproducible plasma discharges were run, one with a nominal core electron density of 1.0×10^{14} cm^{-3}, and the other with a nominal core density of 2.0×10^{14} cm^{-3}. The molybdenum spectra in the 45 to 60-Å range were obtained using a multilayer mirror (MLM) based polychromator [12] built at the Johns Hopkins University. The polychromator had a radial view through the plasma center. The polychromator monitored the wavelength of either the $3d$-$4s$ $E2$ (~59 Å) or $3d$-$4p$ $E1$ (~50 Å) emission during a series of laser injections of molybdenum into the above-mentioned plasmas. Since the ratio of the $3d$-$4s$ $E2$ to $3d$-$4p$ $E1$ emission is desired, a 2.2-m, absolute-intensity calibrated, grazing incidence spectrograph [13] has been used to measure the shot-to-shot variation in the molybdenum emission. The minimum first-order wavelength observable with the grazing incidence spectrometer is 57 Å, hence it is unable to view the Mo^{14+} $E1$ emission, and simultaneous measurement of $3d$-$4p$ $E1$ and $3d$-$4s$ $E2$ emission of Mo^{14+} with this device is impossible. Zirconium was introduced into the plasma to have the longer wavelength Zr^{12+} $3d^{10}$-$3d^9 4p$ $E1$ and

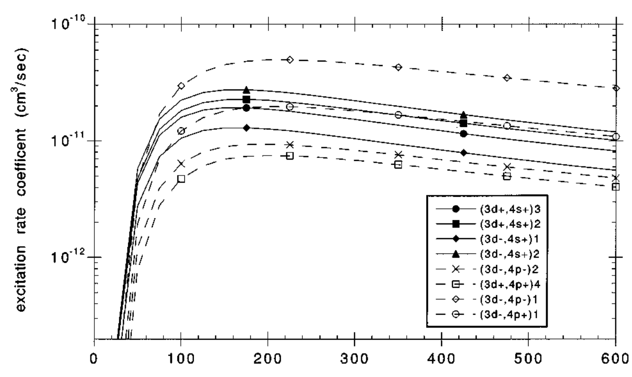

FIG. 1. The resonant excitation rate coefficient as a function of temperature for the four $3d^9 4s$ (solid lines, filled symbols) and four $3d^9 4p$ (dashed, open symbols) levels of Mo^{14+} as computed by Eq. (1). The levels are designated as in Table I.

TABLE I. Comparison of the resonant excitation rate (R) found by Eq. (1) and the direct DWA excitation rate (D) from the ground level to the 16 lowest-energy excited states of Mo^{14+} (in 10^{-13} cm^3/sec). The levels are designated by two jj-coupled orbitals, the first being the $3d$ hole, the second being the occupied, excited orbital, and the total J value for the level, written as a subscript after the parentheses. Each orbital is indicated by "+" or "−" for $l+s$ and $l-s$ coupling. The levels are listed in order of increasing energy.

		Resonant excitation rate coefficient (10^{-13} cm^3 sec^{-1}) Electron temperature (eV)								
Level		50	75	100	125	150	175	200	250	300
$(3d_+,4s_+)_3$	R	43.55	111.6	159.2	183.4	192.2	192.0	186.8	170.6	152.8
	D	6.800	21.36	35.43	45.82	53.23	57.53	60.42	62.13	61.22
$(3d_+,4s_+)_2$	R	47.82	125.3	182.0	212.7	225.3	227.0	222.5	205.3	185.2
	D	17.78	59.80	106.0	146.1	179.1	204.5	225.1	253.4	270.9
$(3d_-,4s_+)_1$	R	27.75	73.05	105.6	122.7	129.3	129.7	126.6	116.1	104.3
	D	2.690	8.650	14.50	18.85	22.02	23.84	25.12	25.90	25.58
$(3d_-,4s_+)_2$	R	58.26	153.9	222.7	259.0	273.1	274.0	267.6	245.6	220.8
	D	20.69	71.69	129.1	179.8	222.2	255.3	282.6	320.7	345.1
$(3d_+,4p_-)_2$	R	13.40	42.83	69.31	86.74	96.31	100.4	101.0	96.76	89.53
	D	3.418	13.32	24.85	34.83	42.49	48.07	51.89	55.97	56.99
$(3d_+,4p_-)_3$	R	16.87	52.46	83.53	103.4	114.0	118.2	118.4	112.7	103.8
	D	5.364	21.44	40.94	58.31	73.12	83.97	93.09	104.6	111.0
$(3d_-,4p_-)_2$	R	12.18	39.36	63.92	80.14	89.07	92.93	93.54	89.63	82.97
	D	2.533	9.945	18.47	25.31	31.12	34.39	37.46	39.94	40.39
$(3d_+,4p_+)_1$	R	24.37	85.69	145.9	188.2	213.1	225.2	228.8	222.1	207.3
	D	1.746	7.006	13.09	17.55	22.82	23.69	30.32	50.37	134.4
$(3d_+,4p_+)_4$	R	7.847	27.86	47.55	61.43	69.64	73.69	74.95	72.87	68.10
	D	4.230	16.71	31.15	42.70	52.67	58.19	63.55	67.86	68.66
$(3d_+,4p_+)_2$	R	6.906	24.60	42.10	54.49	61.87	65.53	66.70	64.91	60.71
	D	1.313	5.276	9.930	13.95	17.01	19.21	20.68	22.15	22.34
$(3d_-,4p_+)_0$	R	3.155	10.74	17.85	22.66	25.38	26.60	26.87	25.85	23.99
	D	0.679	2.776	5.309	7.560	9.321	10.63	11.55	12.57	12.87
$(3d_+,4p_+)_3$	R	6.366	23.56	41.09	53.78	61.50	65.48	66.91	65.47	61.45
	D	3.034	12.66	24.80	36.15	45.65	53.29	59.23	67.42	72.16
$(3d_-,4p_-)_1$	R	46.49	169.1	295.9	390.0	449.2	481.2	494.4	487.9	460.8
	D	34.72	154.3	323.6	504.4	670.3	837.0	960.3	1194	1398
$(3d_-,4p_+)_3$	R	16.05	53.87	89.10	112.9	126.2	132.3	133.6	128.6	119.3
	D	4.384	18.54	36.50	53.12	67.49	78.51	87.71	99.95	107.2
$(3d_-,4p_+)_1$	R	19.51	70.10	121.2	158.2	180.8	192.4	196.7	192.6	180.9
	D	7.990	32.37	68.20	107.9	141.2	173.1	200.4	236.6	218.1
$(3d_-,4p_+)_2$	R	11.96	39.83	65.86	83.46	93.38	97.87	98.84	95.11	88.28
	D	1.081	4.428	8.393	11.79	14.43	16.25	17.54	18.76	18.91

$3d^{10}$-$3d^9 4s$ $E2$ lines appear in the spectrograph's wavelength range. The spectrograph can cover ~30 Å at one time with a spectral resolution of 0.57 Å.

Collisional-radiative (CR) models have been constructed using atomic structure data generated by the HULLAC package [9,14]. Details of the methods used in constructing the CR models have appeared elsewhere [15]. Line emissivities are calculated by multiplying the total radiative transition rate between levels by the population in the upper level. Energy levels from configurations of the form $3p^6 3d^{10}$, $3p^6 3d^9 4l$ $(l=s,p,d,f)$, $3p^6 3d^9 5l$ $(l=s,p,d,f,g)$, $3p^5 3d^{10} 4l$ $(l=s,p,d,f)$, $3p^6 3d^8 4s4l$ $(l=s,p,d,f)$, and $3p^5 3d^9 4s4l$ $(l=s,p,d,f)$ are considered when solving for the level populations.

The ratio of $3d^{10}$-$3d^9 4s$ $E2$ emission to $3d^{10}$-$3d^9 4p$ $E1$ emission for Mo^{14+} and Zr^{12+} is found from the collisional-radiative models by

$$R(n_e,T_e)=\frac{\Sigma_{\text{all } E2 \text{ decays}} I(3d\rightarrow 4s)}{\Sigma_{\text{all } E1 \text{ decays}} I(3d\rightarrow 4p)}, \tag{3}$$

where $I(f\rightarrow i)$ is the emissivity of a transition. R_0 is defined as the value of $R(n_e,T_e)$ at $n_e=1.0\times 10^{13}$ cm^{-3} for a given T_e. Table II contains the values of $R(n_e,T_e)$ from the CR models for Mo^{14+}, which include the full effects of resonant excitation channels and cascades from the $3d^9 5l$ levels.

A. Molybdenum observations

The measured ratio of the Mo^{14+} $E2$-$E1$ emission in the C-Mod experiments is found to be 1.1 ± 0.3 for a plasma with an electron density of 0.6×10^{14} cm^{-3} measured near the last closed magnetic flux surface (LCFS), where the Mo^{14+} ion density is predicted to be maximal, and 1.8 ± 0.5 for a plasma with an electron density of 1.4×10^{14}

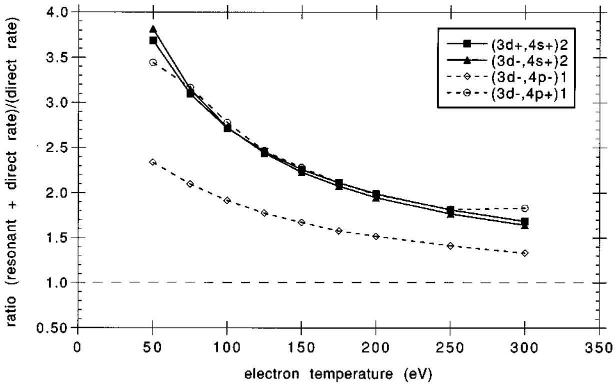

FIG. 2. The factor by which the resonant excitation channels enhance the direct impact-excitation rates into the upper states of the $3d$-$4s$ (solid lines) and $3d$-$4p$ (dashed lines) transitions discussed in Sec. IV. The quantity on the vertical scale is the sum of the resonant plus direct excitation rate, divided by the direct excitation rate. The dashed line at 1.0 represents no enhancement of the direct impact-excitation rates. The levels are designated as in Table I.

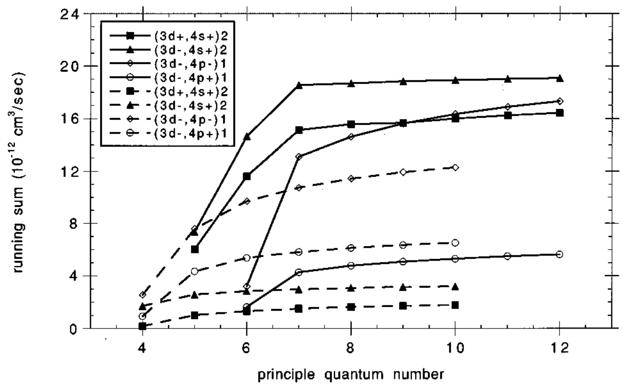

FIG. 3. The running sum of the contribution to the total resonant excitation rate coefficient from each manifold of levels vs the principal quantum number of the manifold. The $3d+e\rightarrow 4ln'l'$ (solid lines) and $3p+e\rightarrow 4ln'l'$ (dashes) channels for the upper states of the $3d$-$4s$ $E2$ and $3d$-$4p$ $E1$ transitions discussed in Sec. III are shown. The levels are designated as in Table I.

cm^{-3} near the LCFS. The 30% uncertainty in the above measurements is the sum of the uncertainty from the photometric calibration of the instrument [12] and the shot-to-shot variation of the molybdenum injection for the wavelength scans.

Because the MLM polychromator used to measure the Mo^{14+} emission was limited to a line of sight through the center of the plasma, the radial position of the emitting shell for the Mo^{14+} ions is not known. Spatial (radial) profiles of the electron temperature in the Alcator C-Mod tokamak are obtained by electron cyclotron emission (ECE) spectra measurements [16]. The electron temperature data in the region of the LCFS are uncertain to $\pm 20\%$ due to poor spatial resolution in the ECE measurements, and are nonexistent in the outermost part of the plasma. Given the measured characteristics of impurity transport in Alcator C-Mod plasmas [17], we can estimate to within a few centimeters the region where Mo^{14+} should emit in the plasma. Radial profiles of the edge electron density are obtained with a reflectometer consisting of five amplitude modulated channels spanning 50–110 GHz [18]. Data from the local density measurements are accurate to $\pm 10\%$ from the scrape-off layer to well inside the LCFS. Given the estimate for the radial position of the Mo^{14+} ion, the measured density profile [18] can be used to describe a range of electron densities seen by the emitting ion.

Klapisch *et al.* [1] have recorded spectra of Mo^{14+} $E1$ and $E2$ lines on film in the Tokamak at Fortney aux Roses (TFR). Although a trace of the observations has been published (Fig. 1 in Ref. [1]), the spectrum is not photometrically calibrated. The published spectrum implies that the Mo^{14+} $E2$ lines are the strongest lines in that portion of the spectrum and that $R(n_e,T_e)\approx 1.4$. Sugar, Reader, and Rowan [19] have recently published a trace of a molybdenum spectrum in the same wavelength range recorded on film in the Texas Experimental Tokamak (TEXT). There, too, the apparent value of $R(n_e,T_e)$ is at least 1.5. Figure 4 shows the calculated $E2$-$E1$ ratio for Mo^{14+} at six temperatures where an appreciable fraction of the molybdenum should exist in the Ni I–like charge state. Also plotted on Fig. 4 are the experimental points from the present observations in Alcator C-Mod and from the TFR observations [1]. The points measured in the present experiments on C-Mod

TABLE II. The value of $R(n_e,T_e)$ in Mo^{14+} from Eq. (3) at nine different free electron densities. Numbers in parentheses represent powers of 10, $X(Y)=X\times 10^{Y}$.

	With resonant excitation, $5l$'s included					
	T_e (eV)					
n_e (cm^{-3})	50	75	100	150	200	300
1.00(13)	2.20	1.64	1.39	1.18	1.07	0.97
5.00(13)	2.13	1.59	1.36	1.15	1.05	0.95
1.00(14)	2.05	1.54	1.31	1.12	1.02	0.93
5.00(14)	1.57	1.21	1.05	0.91	0.84	0.77
1.00(15)	1.22	0.95	0.84	0.74	0.69	0.64
5.00(15)	0.43	0.35	0.32	0.29	0.28	0.27
1.00(16)	0.24	0.20	0.18	0.17	0.16	0.15
5.00(16)	0.05	0.04	0.04	0.04	0.04	0.03
1.00(17)	0.03	0.02	0.02	0.02	0.02	0.02

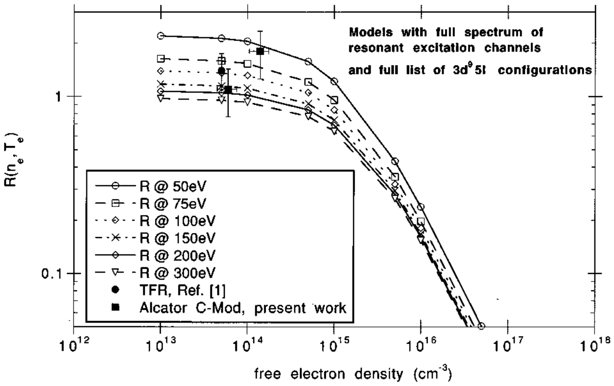

FIG. 4. Plot of $R(n_e,T_e)$ as a function of density for Mo^{14+} showing effects of changes in electron temperature. From top to bottom, the traces are for the $E1$-$E1$ ratio as computed at 50, 75, 100, 150, 200, and 300 eV. The solid points are from measurements by Klapisch *et al.* in TFR (Ref. [1]) and in the Alcator C-Mod tokamak with the instrument described in Ref. [12].

have horizontal error bars corresponding to a 25% uncertainty in the local density due to the uncertainty in the estimated radial position of the Mo^{14+} ion.

The inclusion of the resonant excitation rates in the present models enhances the value of R_0 by nearly 80% at a temperature of 50 eV, and nearly 50% at a temperature of 100 eV (the strength of the effect is a strong function of temperature; see Fig. 2). The model reveals that the presence of the $3d^9 5l$ cascades increases the values of $R(n_e,T_e)$ in Table II by less than 15%; the population flux from ionization-recombination channels from adjacent charge states changes $R(n_e,T_e)$ by less than 5%. The present model for $R(n_e,T_e)$ in Mo^{14+} yields a value closest to the TFR measurement (at a density of 5×10^{13} cm^{-3}, a density appropriate for a TFR plasma) at a temperature near 100 eV. At the reported densities of the present C-Mod experiments, the measured values of the $E2$-$E1$ ratio for Mo^{14+} will obtain (from the curves in Fig. 4) at temperatures between 50 and 150 eV. These temperatures agree well with the predicted ionization-equilibrium temperature of Mo^{14+} of 100 eV [20]. The horizontal error bars on the measured points in Fig. 4 do not change this conclusion. The difference between the two measured values of $R(n_e,T_e)$ for the high and low density shots cannot lead one to conclude there is a significant difference in the plasmas' edge temperature. Without simultaneous measurement of the Mo^{14+} $E2$ and $E1$ emission in the different plasmas, such conclusions are impossible; the introduction of zirconium to the plasma addresses this problem.

B. Zirconium identifications and observations

Figure 5 shows a spectrum recorded with the spectrograph described in Ref. [13] immediately before a zirconium injection into the C-Mod plasma (top frame) and at the peak of the Zr^{12+} emission (middle frame). The spectrum measured by the spectrograph was integrated for 4 msec. The bottom frame in Fig. 5 shows the subtraction of the top and middle frames, and hence, the background from intrinsic impurities in the plasma has been removed yielding a nominally pure zirconium spectrum. Figure 5 also shows a reconstruction of the magnetic flux surfaces in the C-Mod plasma and the

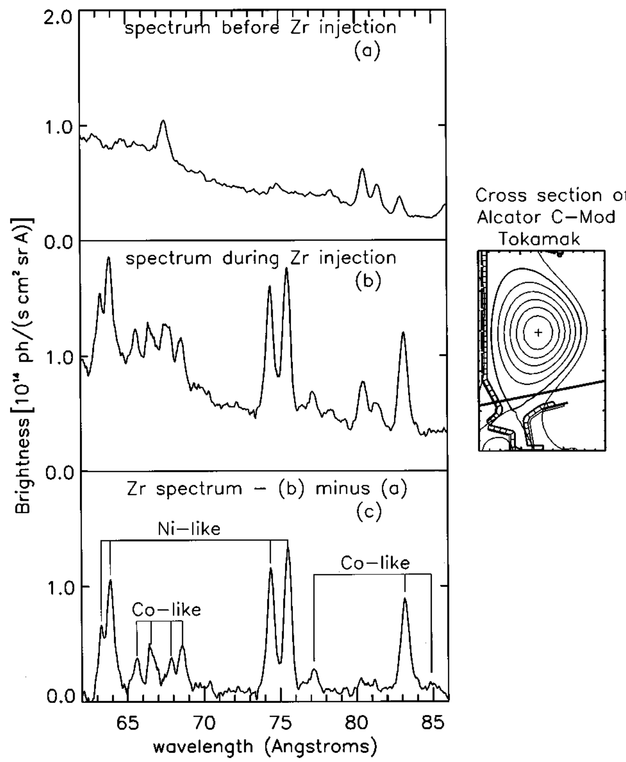

FIG. 5. Spectrum recorded before impurity injection (top), spectrum recorded at peak of impurity emission (middle), and background-subtracted zirconium spectrum (bottom). The frame on the right shows a cross section of the Alcator C-Mod tokamak and reconstructions of the magnetic flux surfaces. The bold line at the bottom of the figure is the line of sight for which the Zr^{12+} emission was observed to be maximal.

viewing chord along which the Zr^{12+} emission was observed to be maximal. The line of sight was scanned (vertically) with a 1.5-cm spatial resolution for several shots, and the position of maximum emission was determined. The Zr^{12+} emission is seen to peak just inside the LCFS.

Table III lists the lines of Zr^{12+} and Zr^{13+} identified in the present work. The wavelength determination has been made by using the following lines: B^{3+} at 60.314 Å, C^{5+} Ly-α in second order at 33.734$\times$2 Å, two C^{4+} lines in second order at 40.268$\times$2 and 40.731$\times$2 Å, Ar^{8+} in second order at 41.48$\times$2 Å and F^{6+} at 86.764 Å. The Zr^{12+} $3d^{10}$-$3d^9 4p$ $E1$ [5] and the Zr^{13+} $\Delta n=0$ $3p^6 3d^9$-$3p^5 3d^{10}$ lines [21] have been observed previously. Table III also lists the brightness observed in the present experiment for each feature. The similarity between the background-subtracted spectrum in the bottom frame of Fig. 5, and the molybdenum spectrum in Fig. 1 of Ref. [19] is worthy of notice. Although the wavelength accuracy in Table III is low compared to spectroscopic work done with photographic plates [19], isoelectronic trends in the spectra of Ni I– and Co I–like molybdenum and zirconium confirm the present identifications.

The RX rate coefficients coupling the ground state of Zr^{12+} to the $3d^9 4s$ and $3d^9 4p$ levels have been found by scaling the *ab initio* calculations for Mo^{14+} according to the behavior of the $\Delta n\geqslant 1$, dipole-allowed radiative decay rates [22]. It is well known that autoionization rates are nearly independent of nuclear charge for intermediate-Z ions, and

TABLE III. Identification of Ni I–like Zr^{12+} $3d$-$4p$ $E1$ and $3d$-$4s$ $E2$ and Co I–like Zr^{13+} $3d$-$4s$ $E2$ lines as measured in the Alcator C-Mod tokamak plasma. Previous measurements in a vacuum spark plasma of the Ni I–like Zr^{12+} $3d$-$4p$ $E1$ [5] and the Co I–like Zr^{13+} $\Delta n=0$ $3p$-$3d$ [21] wavelengths are also reported. The brightness for each feature has been measured in the current experiments with the instrument described in Ref. [13]. Numbers followed by ''blend'' are from a single, unresolved feature in the measured spectrum.

Transition	λ (obs.) (Å)	λ (obs.) (Å)	λ (theor.) (Å)	Brightness[e] [10^{14} photon/(sec cm^2 sr)]
$3d^{10}\ ^1S_0$-$3d^9 4p(^2D_{3/2},3/2)^3D_1$	63.28[a]	63.231[c]	62.902	0.28
$3d^{10}\ ^1S_0$-$3d^9 4p(^2D_{3/2},3/2)^1P_1$	63.89[b]	63.820[c]	63.443	0.59
$3d^9\ ^2D_{5/2}$-$3d^8 4s(^1G_4,1/2)_{9/2}$	65.59[a]		65.218	0.18
$3d^9\ ^2D_{3/2}$-$3d^8 4s(^1G_4,1/2)_{7/2}$	66.54[a]		66.061	0.26
$3d^9\ ^2D_{5/2}$-$3d^8 4s(^3F_3,1/2)_{7/2}$	67.82[a]		67.650	0.17
$3d^9\ ^2D_{5/2}$-$3d^8 4s(^3F_4,1/2)_{7/2}$	68.57(blend)		68.402	0.26(blend)
$3d^9\ ^2D_{3/2}$-$3d^8 4s(^3F_2,1/2)_{5/2}$	68.57(blend)		68.766	0.26(blend)
$3d^9\ ^2D_{5/2}$-$3d^8 4s(^3F_4,1/2)_{9/2}$	68.57(blend)		68.772	0.26(blend)
$3d^{10}\ ^1S_0$-$3d^8 4s(^2D_{3/2},1/2)^1D_2$	74.38[b]		73.985	0.67
$3d^{10}\ ^1S_0$-$3d^9 4s(^2D_{5/2},1/2)^3D_2$	75.51[b]		75.116	0.81
$3p^6 3d^9\ ^2D_{3/2}$-$3p^5 3d^{10}\ ^2P_{1/2}$	77.20[a]	77.249[d]	76.026	0.13
$3p^6 3d^9\ ^2D_{5/2}$-$3p^5 3d^{10}\ ^2P_{3/2}$	83.18[b]	83.196[d]	81.790	0.58
$3p^6 3d^9\ ^2D_{3/2}$-$3p^5 3d^{10}\ ^2P_{3/2}$	84.71[f]	84.621[d]	83.131	0.06

[a]Accuracy ±0.04 Å.
[b]Accuracy ±0.01 Å.
[c]E. Alexander *et al.*, J. Opt. Soc. Am. **61**, 508 (1971). Accuracy ±0.005 Å.
[d]A. Ryabstev and J. Reader, J. Opt. Soc. Am. **72**, 710 (1982). Accuracy ±0.005 Å.
[e]Uncertainty ±15%.
[f]Accuracy ±0.5 Å.

that $\Delta n \geqslant 1$, dipole-allowed radiative rates scale as Z_c^4, where Z_c is the charge seen by the electron undergoing the transition [22]. Table IV lists the model values of $R(n_e,T_e)$ as a function of n_e at the five temperatures. The inclusion of the RX rates in the CR model for Zr^{12+} enhances the value of $R(n_e,T_e)$ significantly; the value of R_0 is enhanced by 65% at $T_e=40$ eV, by greater than 50% at $T_e=50$ eV, and by 30% at $T_e=100$ eV.

Figure 6 shows the curves of $R(n_e,T_e)$ for Zr^{12+} calculated from Eq. (3) at five temperatures and the value of $R(n_e,T_e)=1.69\pm0.24$ found for Zr^{12+} in the present experiments. The spatial resolution of the instrument used to measure $R(n_e,T_e)$ allows the location of the region from which the Zr^{12+} ions emit in the plasma to be known to ≈1 cm. Hence, we can use the measured electron density profile [18] in C-Mod directly to place this point on the ordinate of Fig. 6; the local electron density seen by the Zr^{12+} ion, 0.9×10^{14} cm^{-3}, is shown with a ±10% horizontal error bar. The 15% uncertainty in the measured $R(n_e,T_e)$ value for Zr^{12+} comes from the uncertainty in the photometric calibration of the spectrograph [13] and uncertainties in the fits to the line shapes.

TABLE IV. The value of $R(n_e,T_e)$ in Zr^{12+} from Eq. (3) at nine different free electron densities. Numbers in parentheses represent powers of 10, $X(Y)=X\times10^Y$.

	With resonant excitation, 5*l*'s included				
	T_e (eV)				
n_e (cm^{-3})	40	50	75	100	150
1.00(13)	2.30	1.91	1.46	1.25	1.04
5.00(13)	2.11	1.76	1.36	1.16	0.98
1.00(14)	1.91	1.60	1.25	1.07	0.91
5.00(14)	1.08	0.93	0.75	0.67	0.59
1.00(15)	0.70	0.61	0.50	0.45	0.41
5.00(15)	0.18	0.16	0.14	0.13	0.12
1.00(16)	0.09	0.08	0.07	0.07	0.07
5.00(16)	0.02	0.02	0.01	0.01	0.01
1.00(17)	0.00	0.00	0.00	0.00	0.00

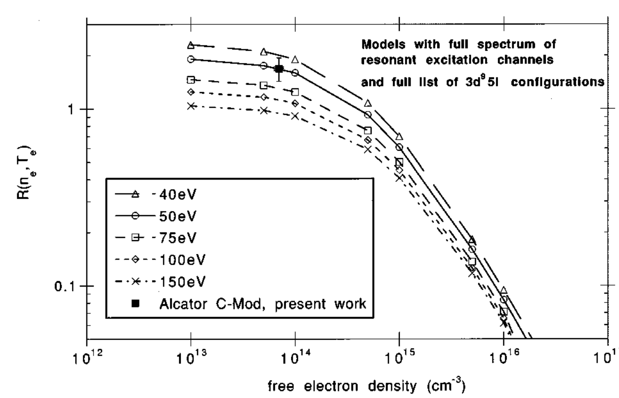

FIG. 6. Plot of $R(n_e,T_e)$ as a function of density for Zr^{12+} showing effects of changes in electron temperature. From top to bottom, the traces are for the $E2$-$E1$ ratio as computed at 40, 50, 75, 100, and 150 eV. The solid points are from measurements in the Alcator C-Mod tokamak with the instrument described in Ref. [13].

From the curves in Fig. 6, the measured value of $R(n_e, T_e)$ implies the Zr^{12+} ion emits from a region of the plasma with T_e between 50 and 75 eV. There are no accurate measurements of the local electron temperature in C-Mod at this radius. However, the reduction in the local temperature for Zr^{12+} (50 eV) derived from Fig. 6 compared to the local temperature for Mo^{14+} (100 eV) derived from Fig. 4 is consistent with expected Z scaling of ionization potentials [22].

IV. CONCLUSIONS

Detailed calculations have been performed for the rate of resonant excitation into the $3d^9 4s$ and $3d^9 4p$ levels of Mo^{14+}. The calculations were scaled isoelectronically to provide the equivalent data for Zr^{12+}. The process of resonant excitation has been found to have a large effect on the $3d^{10}$-$3d^9 4s$ $E2$ and $3d^{10}$-$3d^9 4p$ $E1$ transitions, which dominate the soft x-ray spectra of Mo^{14+} and Zr^{12+}. The inclusion of the resonant channels from the ground state of the Ni I-like ion to the levels of the first two excited configurations greatly enhances the value of the predicted $E2$-$E1$ emission ratio at temperatures at or below these ions' ionization-equilibrium temperatures. Further, enhanced diagnostic potential is found for this system of transitions because the inclusion of the resonant excitation channels introduces temperature sensitivity into the ratio. Calculations made for low-density plasmas indicate that if either the local temperature or density is known, these ions can serve as robust diagnostics of the remaining plasma parameter.

ACKNOWLEDGMENTS

The authors would like to thank the staff at the Plasma Fusion Center, Massachusetts Institute of Technology, for their help in conducting the experiments in this paper. The present work was performed under the auspices of the U.S. Department of Energy by contract between the Plasma Spectroscopy Group at Johns Hopkins University and the Lawrence Livermore National Laboratories under Contract No. W-7405-ENG-48.

[1] M. Klapisch, J. Schwob, M. Finkenthal, B. Fraenkel, S. Egert, A. Bar-Shalom, C. Breton, C. DeMichelis, and M. Mattioli, Phys. Rev. Lett. **41**, 403 (1978).

[2] S. Maxon, P. Hagelstein, J. Scofield, and Y. Lee, J. Appl. Phys. **59**, 293 (1986).

[3] B. J. MacGowen, S. Maxon, P. Hagelstein, C. Keane, R. London, D. Mathews, M. Rosen, J. Scofield, and A. Whelan, Phys. Rev. Lett. **59**, 2157 (1987).

[4] M. Chen and K. Reed, Phys. Rev. A **40**, 2292 (1989); W. H. Goldstein, A. L. Osterheld, J. Oreg, and A. Bar-Shalom, Astrophys. J. **344**, L37 (1989).

[5] E. Alexander, M. Even-Zohar, B. Fraenkel, and S. Goldsmith, J. Opt. Soc. Am. **61**, 508 (1971).

[6] J. L. Schwob, M. Klapisch, N. Schweitzer, M. Finkelthal, C. Breton, C. DeMichelis, and M. Mattioli, Phys. Lett. **62A**, 85 (1977).

[7] M. Klapisch, E. Meroz, P. Mandelbaum, A. Zigler, C. Bauche-Arnoult, and J. Bauche, Phys. Rev. A **25**, 2391 (1982).

[8] M. W. D. Mansfield, N. J. Peacock, C. C. Smith, M. G. Hobby, and R. D. Cowan, J. Phys. B **11**, 1521 (1978).

[9] M. Klapisch, Comput. Phys. Commun. **2**, 239 (1971); M. Klapisch, J. L. Schwob, B. S. Fraenkel, and J. Oreg, J. Opt. Soc. Am. **67**, 148 (1977).

[10] J. Oreg, W. H. Goldstein, P. Mandelbaum, D. Mitnik, E. Meroz, J. Schwob, and A. Bar Shalom, Phys. Rev. A **44**, 1741 (1991); J. Oreg, W. H. Goldstein, and M. Klapisch, *ibid.* **4**, 1750 (1991).

[11] I. H. Hutchinson *et al.*, Phys. Plasmas **1**, 1511 (1994).

[12] M. May, M. Finkelthal, S. Regan, H. W. Moos, J. Terry, M. Graf, K. Fournier, and W. H. Goldstein, Rev. Sci. Instrum. **66**, 561 (1995); M. May, A. Zwicker, H. W. Moos, M. Finkelthal, and J. Terry, *ibid.* **63**, 5176 (1992).

[13] J. L. Terry, H. L. Manning, and E. S. Marmar, Proc. SPIE **689**, 54 (1986).

[14] A. Bar-Shalom, M. Klapisch, and J. Oreg, Phys. Rev. A **38**, 1773 (1988).

[15] K. B. Fournier, W. H. Goldstein, D. Pacella, R. Bartiromo, M. Finkelthal, and M. May, Phys. Rev. E **53**, 1084 (1996).

[16] A. E. Hubbard, J. Irby, P. J. O'Shea, P. Stek, V. M. Thannickal, and R. L. Watterson, Bull. Am. Phys. Soc. **40**, 1698 (1995).

[17] M. A. Graf, J. E. Rice, J. L. Terry, E. S. Marmar, J. A. Goetz, G. M. McCracken, F. Bombarda, and M. J. May, Rev. Sci. Instrum. **66**, 636 (1995).

[18] P. Stek, J. Irby, C. Christensen, S. Horne, B. Labombard, E. Marmar, J. Reardon, Y. Takase, and R. Watterson, Bull. Am. Phys. Soc. **40**, 1698 (1995).

[19] J. Sugar, J. Reader, and W. Rowan, Phys. Rev. A **51**, 835 (1995).

[20] D. Mitnik, P. Mandelbaum, J. Schwob, A. Bar-Shalom, J. Oreg, and W. H. Goldstein, Phys. Rev. A **50**, 4911 (1994).

[21] A. Ryabtsev and J. Reader, J. Opt. Soc. Am. **72**, 710 (1982).

[22] R. D. Cowan, *The Theory of Atomic Spectra and Structure* (Univ. of California Press, Berkeley, CA, 1981).